Journal of Energy Chemistry 26 (2017) 200–206

Contents lists available at ScienceDirect

Journal of Energy Chemistry

journal homepage: www.elsevier.com/locate/jechem

http://www.journals.elsevier.com/journal-of-energy-chemistry/

Wormholelike mesoporous carbon supported PtRu catalysts toward methanol electrooxidation

Weifeng Liu[a,b], Xiaoping Qin[b], Xiongfu Zhang[a,*], Zhigang Shao[b], Baolian Yi[b]

[a] State Key Laboratory of Fine Chemicals, School of Chemical Engineering, Dalian University of Technology, Dalian 116024, Liaoning, China
[b] Dalian Institute of Chemical Physics, Chinese Academy of Sciences, Dalian 116023, Liaoning, China

ARTICLE INFO

Article history:
Received 12 June 2016
Revised 5 July 2016
Accepted 6 July 2016
Available online 4 August 2016

Keywords:
Wormholelike mesoporous carbon
PtRu catalyst
Pore diameter
Methanol electrooxidation

ABSTRACT

Wormholelike mesoporous carbons (WMCs) with three different pore diameters (D_p), namely WMC-F7 ($D_p = 8.5$ nm), WMC-F30 ($D_p = 4.4$ nm), and WMC-F0 ($D_p = 3.1$ nm) are prepared via a modified sol–gel process. Then PtRu nanoparticles with the particle size (d_{Pt}) of ~3.2 nm supported on WMCs are synthesized with a modified pulse microwave-assisted polyol method. It is found that the pore diameter of WMCs plays an important role in the electrochemical activity of PtRu toward alcohol electrooxidation reaction. PtRu/WMC-F7 with $D_p > 2d_{Pt}$ exhibits the largest electrochemical surface area (ESA) and the highest activity toward methanol electrooxidation. With the decrease in D_p, PtRu/WMC-F30 and PtRu/WMC-F0 have much lower ESA and electrochemical activity, especially for the isopropanol electrooxidation with a larger molecular size. When D_p is more than twice d_{Pt}, the mass transfer of reactants and electrolyte are easier, and thus more PtRu nanoparticles can be utilized and the catalysts activity can be enhanced.

1. Introduction

Due to the facile storage and refilling characteristics of methanol, direct methanol fuel cells (DMFCs) possess the advantages of simple structure and high energy density, which makes them potentially the portable power packs or micro-powers for domestic appliances [1,2]. However, the commercial applications of DMFCs are mainly hindered by the sluggish kinetics of methanol electrooxidation reaction (MOR), the easy poison to CO-like species of electrocatalysts, and methanol crossover from the anode to the cathode through the electrolyte membranes. In recent years, the development of key materials (electrocatalysts and electrolyte membranes) and core technologies (electrode preparation and membrane electrode assembly fabrication) have provided many ideas for resolving above problems. Pt based materials supported on carbon, such as PtRu/C, PtIr/C, PtRuIr/C, PtRhPd/C [3–7] exhibit improved MOR activity and CO tolerance, which have attracted great research interest. Among them, PtRu/C is well recognized as the best catalyst for MOR because of the well-known bi-functional mechanism that Pt adsorbs and oxidizes methanol, and Ru dissociates water at low potentials to form Ru–OH groups which can facilitate conversion of the poisonous CO or CO-like intermediates adsorbed on Pt into CO_2, thereby releasing the catalytic active sites [8–10].

Recently, mesoporous carbons have attracted wide concerns due to their better mass transfer properties. These mesoporous carbons have demonstrated excellent performance in supercapacitors [11,12] and electrocatalyst supports [13,14]. Among the recent developed mesoporous carbons, wormholelike mesoporous carbons (WMCs) have the specific three-dimensional network structure, large surface area and high pore volume, which have been used in the electrode for water purification, and gas separation [15]. After carbonization at high temperature, WMCs have high conductivity and good stability, which makes them as an ideal support for PtRu nanoparticles.

Especially, after Wu et al. [16] realized the easy control of the pore diameter by just changing the HF amount as the catalyst in the sol–gel process of tetraethyl orthosilicate, the application of WMCs have attracted more concerns. Herein, we synthesized WMCs with different pore diameters using a modified sol–gel process. And then, WMCs supported PtRu catalysts were obtained by a modified pulse microwave assisted polyol method and their corresponding physico-chemical and electrochemical performance for MOR were systematically evaluated and analyzed.

2. Experimental

2.1. Preparation of WMCs

According to the reported method, a typical WMCs preparation procedure was described as follows. A pre-calculated quantity of

* Corresponding author. Fax: +86 411 84986155.
E-mail addresses: xfzhang@dlut.edu.cn (X. Zhang), zhgshao@dicp.ac.cn (Z. Shao).

http://dx.doi.org/10.1016/j.jechem.2016.08.003

sucrose was dissolved in H_2SO_4 aqueous solution (pH = 2.0) followed by adding tetraethyl orthosilicate (TEOS) with the ratio of sucrose:H_2SO_4 solution:TEOS = 2 g:3.0 mL:4.0 mL. A homogeneous mixture was obtained after a continuously magnetic stirring. Subsequently, 4.0 wt% hydrofluoric acid (HF) solution (HF/TEOS molar ratio = 1/30) was added under stirring. The obtained homogeneous mixture was gelated and aged in an open plastic bottle at 40 °C for 2 days. The resulting composites were further treated at 100 °C for 6 h and subsequently at 160 °C for another 6 h. And then the sample was heated to 900 °C at a heating rate of 5 °C/min, and kept at 900 °C for 3 h in N_2 flow. After that, the carbon/silica composites were washed using HF solution to obtain WMCs. The different pore diameters of WMCs were controlled by changing the HF content with HF/TEOS molar ratio = 0, 1/30, and 1/7 for WMC-F0, WMC-F30, and WMC-F7, respectively.

2.2. Preparation of PtRu/WMCs

PtRu@WMCs with a Pt loading of 20 wt% and a Ru loading of 10 wt% were prepared by a modified pulse microwave-assisted polyol method [17]. The detailed process includes the following steps. The as-prepared WMCs with different pore diameters were well mixed with ethylene glycol (EG) in an ultrasonic bath respectively, and then an appropriate amount of $H_2PtCl_6{\cdot}6H_2O$ and $RuCl_3$ dissolved in EG was added into the mixture. After the pH value of the above mixture was adjusted to 13 by the dropwise addition of 1.0 mol/L NaOH/EG solution, the well-dispersed slurry was obtained with magnetic stirring for another 1 h. Next, the slurry was microwave-heated in the pulse form of 10 s-ON/10 s-OFF for five times. After re-acidified by 1.0 mol/L HCl to pH = 3.0, the resulting sample was filtered, washed with abundant hot water until no chloride anion was detected by 1.0 mol/L $AgNO_3$ solution in the filtrate. Finally, the sample was obtained after dried at 80 °C overnight in a vacuum oven. According to the used WMCs, the corresponding supported catalysts were denoted as PtRu@WMC-F0, PtRu@WMC-F30, and PtRu@WMC-F7, respectively.

2.3. Characterization of materials

2.3.1. Physico-chemical characterization

The X-ray diffraction (XRD) patterns were obtained on a D-MAX2200VPC diffractometer using Cu *Kα* radiation (30 kV, 30 mA). N_2 adsorption–desorption measurements were carried out on a Micromeritics ASAP2010 analyzer at 77 K. The BET surface area (S_{BET}) and the mesopore volume (V_{mes}) were determined by BET theory and Barrett–Joyner–Halenda (BJH) method, respectively. Scanning electron microscopy (SEM) and element mapping were performed using Quatnta400F thermal field emission environmental SEM. The transmission electron microscopy (TEM) investigations were performed on a JEOL TEM-2010(HR) operating at 120 kV.

2.3.2. Electrochemical characterization

The electrochemical tests were carried out on an AUT84480 instrument in a three-electrode cell. A saturated calomel electrode (SCE) and a Pt foil were used as the reference and counter electrode, respectively. The thin catalyst film was prepared onto the glassy carbon (GC) disk surface (d = 0.5 cm). Typically, a mixture containing 10.0 mg electrocatalyst, 0.9 mL ethanol and 0.1 mL Nafion solution (5 wt%, DuPont Company) was ultrasonicated for 15 min and then stirred for 30 min to obtain a well-dispersed ink. The catalyst ink (10 μL) was then quantitatively transferred onto the surface of the GC electrode and dried under infrared lamp to obtain a catalyst thin film. The Pt loading was 101.9 μg/cm^2. All the potential was referred to the SCE without special specification.

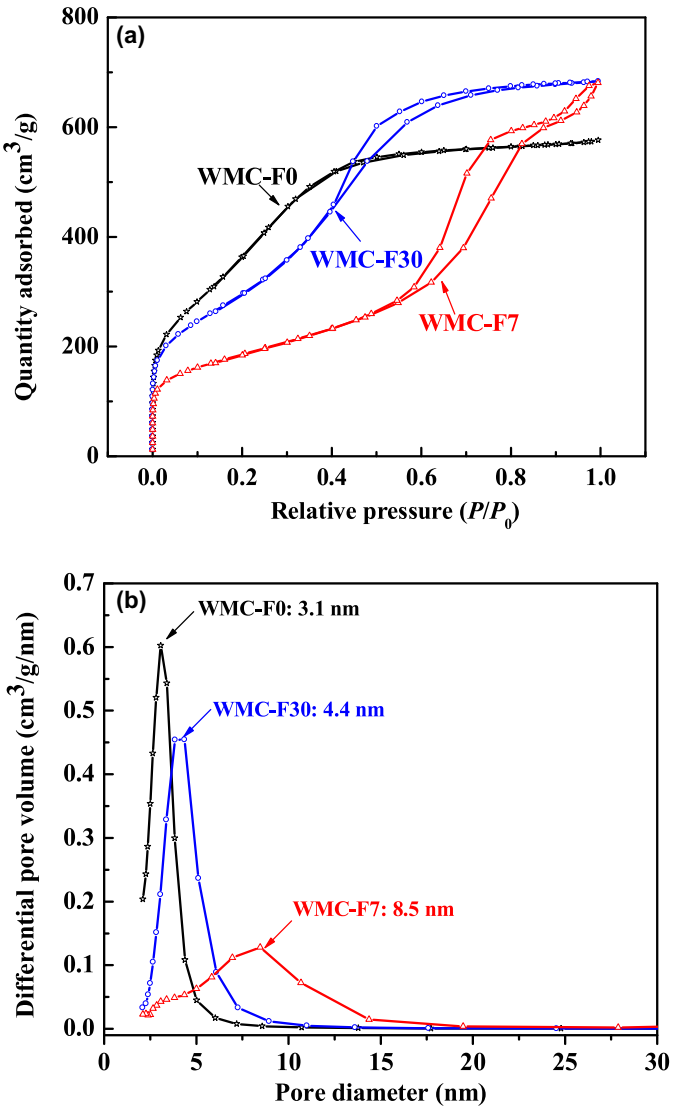

Fig. 1. N_2 adsorption–desorption curves (a) of WMCs with different pore sizes and their corresponding pore size distributions (b).

For the electrocatalytic activity evaluation, the electrochemical tests were performed in 0.5 mol/L H_2SO_4 for electrochemical surface area (ESA) measurements and in 0.5 mol/L H_2SO_4 + 1.0 mol/L CH_3OH for MOR activity by cyclic voltammetry (CV). Before each experiment, the electrolyte solution was bubbled with high-purity N_2 for 30 min to remove the dissolved oxygen inside. Before each test, the working electrodes were electrochemically cleaned by continuous cycling at a scan rate of 50 mV/s until a stable response was obtained.

3. Results and discussion

The pore structures of WMCs were investigated by N_2 adsorption–desorption tests and the results are shown in Fig. 1. Typical IV nitrogen adsorption–desorption isotherms with distinct hysteretic loops indicate the mesoporous structure of all the as-prepared samples (Fig. 1a). The mesoporous size distributions are centered at 3.1 nm, 3.4 nm and 8.5 nm for WMC-F0, WMC-F30 and WMC-F7, respectively (Fig. 1b). The corresponding BET surface areas of the above three samples are 1372 m^2/g for WMC-F0, 1077 m^2/g for WMC-F30, and 659 m^2/g for WMC-F7. Obviously, all these three samples possess the desired mesoporous structure

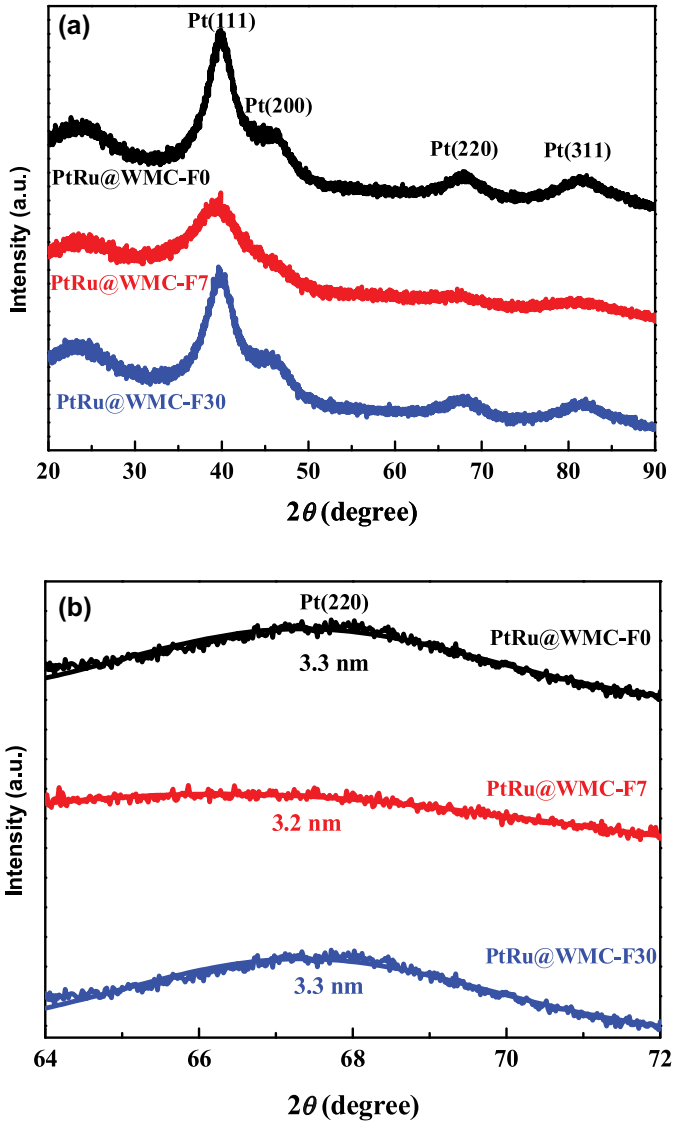

Fig. 2. XRD of the PtRu supported on WMCs with different pore diameters. (a) 2θ scanning range of 20°–90° at a scan rate of 10 °/min, (b) 2θ scanning range of 64°–72° at a scan rate of 1 °/min.

with a large specific surface area, which is beneficial for supporting metal particles with high dispersion.

Fig. 2 displays the XRD results of PtRu@WMCs with different pore diameters. As clearly seen, all samples exhibit the typical characteristics of a crystalline face centered cubic structure of Pt. The fitted (220) plane of Pt was used to calculate the average particle size of metal nanoparticles according to Scherrer formula (Eq. (1)) [18].

$$d = \frac{0.89\lambda_{k\alpha 1}}{B\cos\theta} \quad (1)$$

where d is the particle size of Pt, $\lambda_{k\alpha 1}$ is the X-ray wavelength with the value of 1.54056 Å, B is the line broadening at half the maximum intensity in radians and θ is the Bragg angle.

Based on Fig. 2(b) and Eq. (1), the average Pt particle size for these three samples is almost the same (3.3 nm for both PtRu@WMC-F0 and PtRu@WMC-F30, and 3.2 nm for PtRu@WMC-F7) (Table 1).

Further investigation by TEM (Fig. 3) confirms the similar particle size of PtRu particles, which are evenly dispersed on the WMCs. The high metal dispersion could be attributed to the large specific surface area of WMCs. It indicates that if the surface area of the support materials is big enough, the further increase in the surface area could not obviously affect the metal dispersion. The very similar metal particle size is good for the further electrochemical performance comparison of different WMCs supported PtRu catalysts by eliminating the possible effect of metal particle size.

Table 1. The pore structure parameters of the WMCs and the properties of their corresponding supported PtRu catalysts.

Sample	D_p[a] (nm)	S_{BET} (m^2/g)	d_{Pt}[b] (nm)	I_{fp}[c] (mA/cm^2)	I_{bp}[d] (mA/cm^2)
PtRu@WMC-F7	8.5	659	3.2	37.5	33.0
PtRu@WMC-F30	4.4	1077	3.3	21.6	16.5
PtRu@WMC-F0	3.1	1372	3.3	19.7	13.9

[a] D_p: pore diameter of WMCs.
[b] d_{Pt}: the average metal particle size.
[c] I_{fp}: MOR peak current density in the forward scanning direction.
[d] I_{bp}: MOR peak current density in the backward scanning direction.

The cyclic voltammetric curves of PtRu@WMCs catalysts in N_2-saturated 0.5 mol/L H_2SO_4 are shown in Fig. 4. Obviously, these three investigated catalysts present similar CV curves while a little different from the typical desorption and adsorption peaks of hydrogen on Ptcatalyst [19,20]. From the region marked by the dashed line (Fig. 4), a semi-quantitative evaluation for the electrochemical surface area (ESA) can be obtained. It is clear that PtRu@WMC-F7 has a bigger ESA than PtRu@WMC-F30 and PtRu@WMC-F0. For these three catalysts, the size of metal particle is similar as obtained from XRD and TEM characterizations, thus their difference in ESA could be mainly due to the different pore diameters of WMCs, which directly affects the utilization of metals.

PtRu@WMC-F0, PtRu@WMC-F30, and PtRu@WMC-F7 catalysts were evaluated for MOR by CV technique in 0.5 mol/L H_2SO_4 + 1.0 mol/L CH_3OH at a potential sweeping rate of 50 mV/s. It can be found that PtRu@WMC-F0, PtRu@WMC-F30, and PtRu@WMC-F7 show the similar CV results with very prominent characteristic peaks for MOR. It is generally accepted that there are two steps involved in MOR: (1) methanol is dissociated and then adsorbed onto Pt to produce CO or CO-like intermediates, and (2) the intermediates are further oxidized to CO_2 [21]. Accordingly, in the forward scanning, the oxidation peak in CV curve corresponds to methanol oxidation, and in the backward scanning, the adsorbed intermediates are removed by oxidation, which shows another oxidation peak. The oxidation peak current densities in the forward (I_{fp}) and backward (I_{bp}) scanning on PtRu@WMC-F7 are 37.5 and 33.0 mA/cm^2, which are much higher than the corresponding values on PtRu@WMC-F30 and PtRu@WMC-F0 (Fig. 5a and Table 1). This could be due to the fact that when the pore diameter of WMCs (D_p) is twice the particle size of Pt (d_{Pt}), the ESA and the Pt utilization efficiency are significantly enhanced. Whereas, in the case of $d_{Pt} \le D_p < 2d_{Pt}$, the metal particles in the pores of WMCs could not be accessible by both electrolyte and reactants, thus leading to a deteriorated MOR activity. Moreover, along with the increase in D_p, the easier mass transport can also be beneficial for superior activity for MOR as discussed below. Based on the above results, obviously, WMC-F7 (D_p = 8.7 nm) provides PtRu with the best electrocatalytic activity toward MOR compared with WMC-F30 and WMC-F0. As the potential electrocatalyst support, it is vital to compare its performance with the widely used commercial carbon support material, XC-72 carbon (Cabot Corp.). For comparison, PtRu@XC-72 C catalyst was also prepared following the same catalyst preparation procedure as PtRu@WMC-F7. From Fig. 5(b), it can be distinguished that PtRu@WMC-F7 exhibits comparable and even superior MOR activity to PtRu@XC-72 C. This could be resulted from that the WMC-F7 with higher BET surface

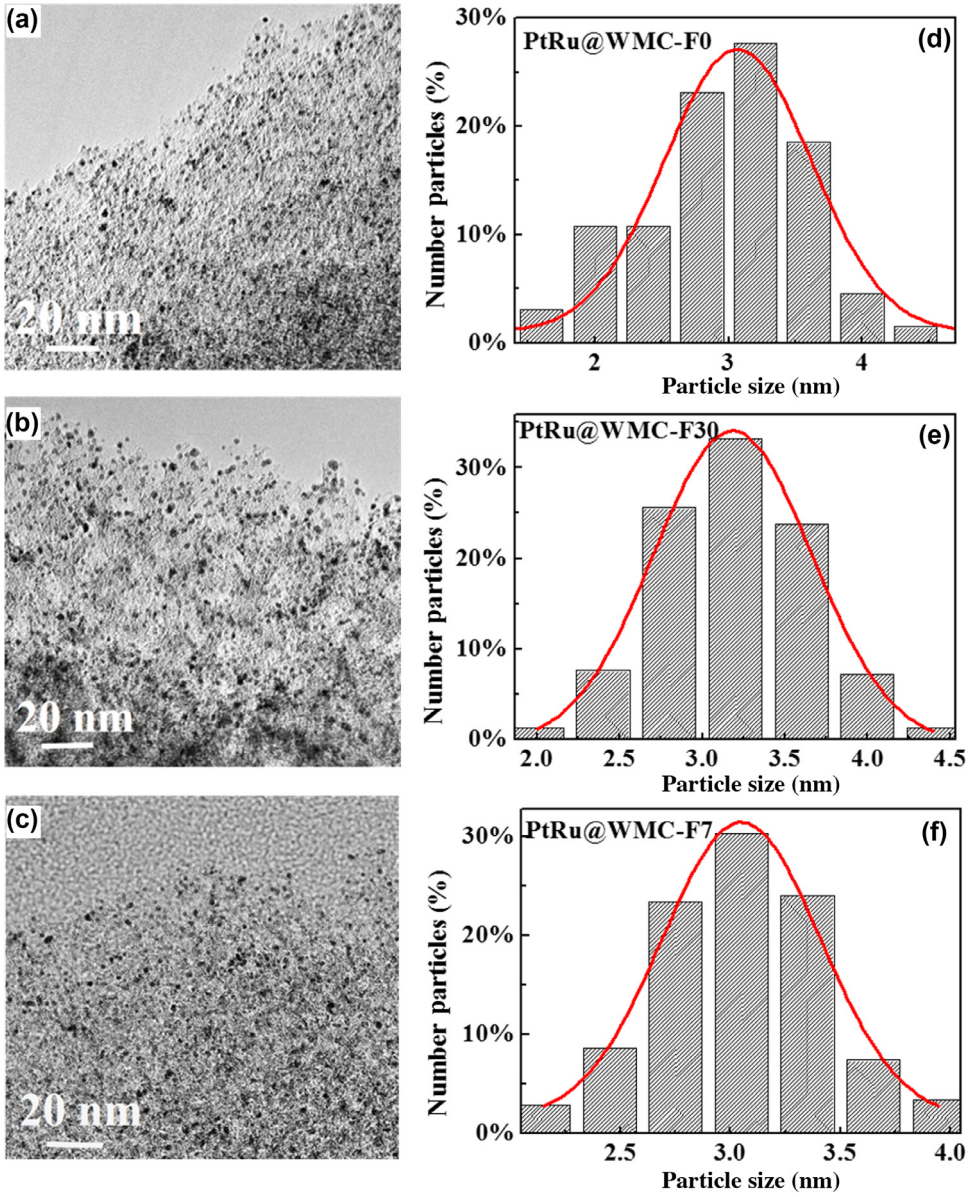

Fig. 3. TEM images of PtRu@WMC-F0 (a), PtRu@WMC-F30 (b), and PtRu@WMC-F7 (c); and their corresponding size distribution histograms PtRu@WMC-F0 (d), PtRu@WMC-F30 (e), and PtRu@WMC-F7 (f).

area (657 m^2/g) provides better metal dispersion than XC-72 carbon (~250 m^2/g).

To further investigate the effect of pore diameter of WMCs on the mass transport and the electrochemical performance of WMC supported PtRu catalysts, two sets of experiments were designed and carried out: (1) CV curves on PtRu@WMC-F0, PtRu@WMC-F30, and PtRu@WMC-F7 in 0.5 mol/L H_2SO_4 + 1.0 mol/L CH_3OH at two different temperatures of 30 °C and 60 °C, and (2) the electrochemical activity toward different alcohol oxidation at the same temperature in the corresponding aqueous solutions of 0.5 mol/L H_2SO_4 + 1.0 mol/L CH_3OH, 0.5 mol/L H_2SO_4 + 1.0 mol/L C_2H_5OH, and 0.5 mol/L H_2SO_4 + 1.0 mol/L $(CH_3)_2CHOH$. As shown in Fig. 6, along with the temperature increment, the MOR activity on PtRu@WMC-F7 is enhanced while there is almost no change for the other two cases of PtRu@WMC-F30 and PtRu@WMC-F0. For a more detailed description as summarized in Table 2, the peak current density for MOR on PtRu@WMC-F7 at 60 °C is almost four times the corresponding value at 30 °C. While on both PtRu@WMC-F30 and PtRu@WMC-F0, there is no improvement in MOR activity when the temperature is increased. This is probably due to that the mass transport of reactants and electrolyte are much more difficult at the case of small D_p.

Table 2. The peak current density of methanol oxidation on PtRu catalysts supported on WMCs with different pore sizes at different temperatures.

Sample	I_p at 30 °C (mA/cm^2)	I_p at 60 °C (mA/cm^2)	r^* (I_p at 60 °C/I_p at 30 °C)
PtRu@WMC-F7	44.0	170.2	3.9
PtRu@WMC-F30	34.9	99.3	2.8
PtRu@WMC-F0	19.7	56.0	2.8

* r: the ratio between the MOR peak current densities at 60 °C and 30 °C.

The further investigation of the effect of D_p of WMCs can be seen in Fig. 7. It can be distinguished that PtRu@WMC-7 exhibits higher activity toward all of the investigated alcohol reactions than PtRu@WMC-F30 and PtRu@WMC-F0, and this superiority becomes more significant for ethanol electrooxidation reaction (EOR) and especially isopropanol electrooxidation reaction (IPOR). Obviously,

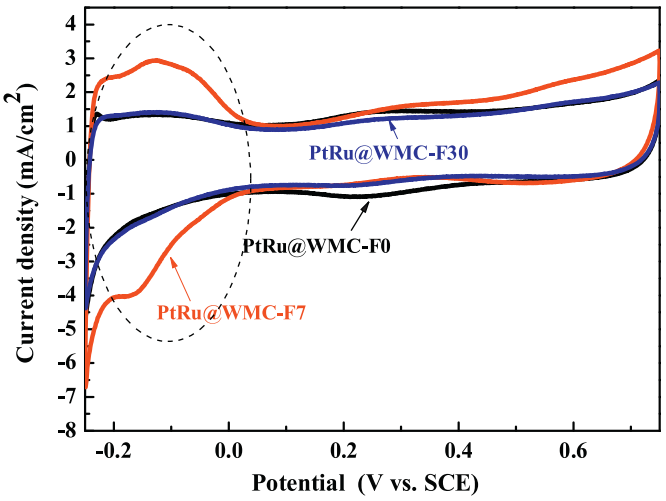

Fig. 4. CVs of PtRu@WMC-F0, PtRu@WMC-F30 and PtRu@WMC-F7 in N_2-saturated 0.5 mol/L H_2SO_4 aqueous solution. Scan rate: 20 mV/s.

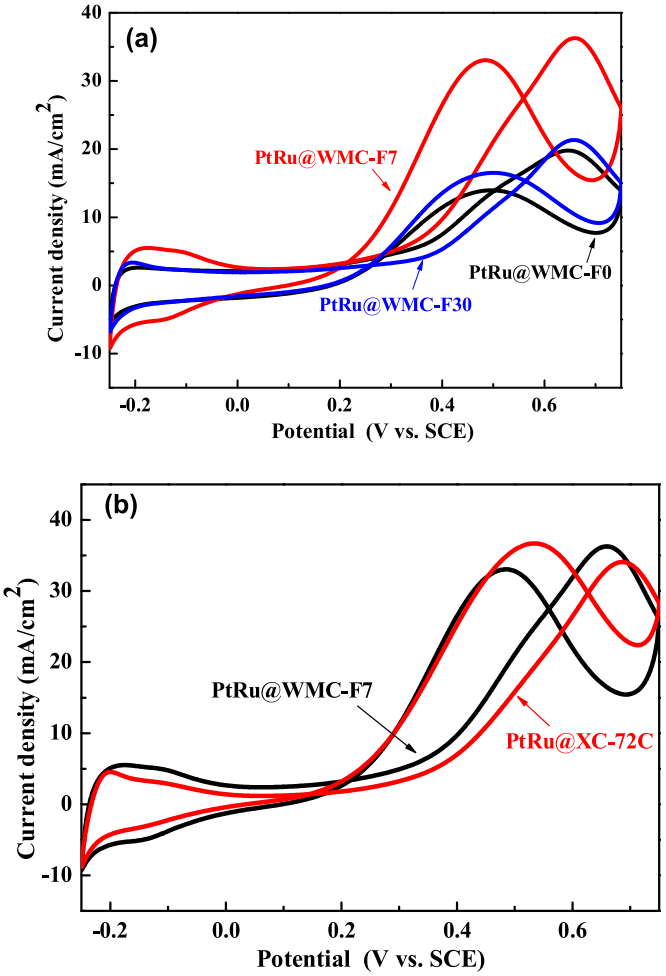

Fig. 5. CVs of PtRu@WMC-F0, PtRu@WMC-F30 and PtRu@WMC-F7 catalysts (a), and the methanol oxidation activity comparison on PtRu@WMC-F7 and PtRu@XC-72C (b), in 0.5 mol/L H_2SO_4 aqueous solution containing 1.0 mol/L CH_3OH at a scan rate of 50 mV/s at 25 °C.

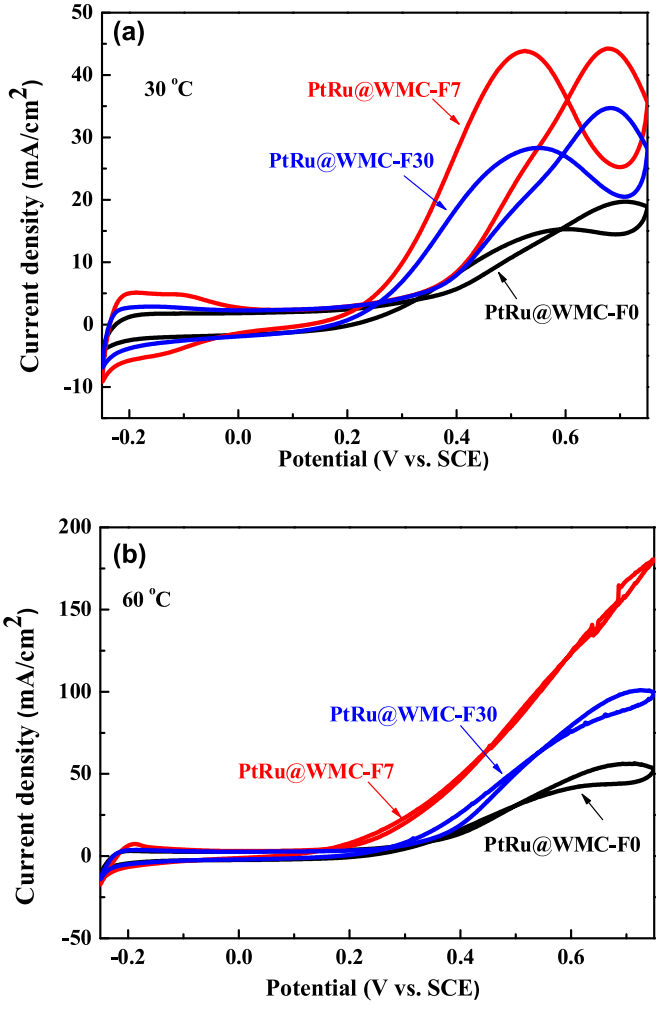

Fig. 6. CVs of PtRu@WMC-F0, PtRu@WMC-F30 and PtRu@WMC-F7 catalysts in 0.5 mol/L H_2SO_4 aqueous solution containing 1.0 mol/L CH_3OH at a scan rate of 50 mV/s at 30 °C (a) and 60 °C (b), respectively.

WMC-F7 with bigger pore diameter can provide PtRu with superior activity for alcohol electrooxidation compared with WMC-F30 and WMC-F0. To quantitatively analyze the superiority of PtRu@WMC-F7, the gain ratio (r_1 and r_2) is defined as Eqs. (2) and (3).

$$r_1 = [I_p(\text{PtRu@WMC} - \text{F7}) - I_p(\text{PtRu@WMC} - \text{F30})/I_p(\text{PtRu@WMC} - \text{F30})] \times 100\% \quad (2)$$

$$r_2 = [I_p(\text{PtRu@WMC} - \text{F7}) - I_p(\text{PtRu@WMC} - \text{F0})/I_p(\text{PtRu@WMC} - \text{F0})] \times 100\% \quad (3)$$

where r_1 is the gain ratio between PtRu@WMC-F7 and PtRu@WMC-F30 for different alcohol electrooxidations, r_2 is the gain ratio between PtRu@WMC-F7 and PtRu@WMC-F0 for different alcohol electrooxidations, and I_p is the peak current density for alcohol electrooxidation in the forward scanning.

As summarized in Table 3 and shown in Fig. 8, it can be distinguished that the respective r_1 value for MOR, EOR, and IPOR are 69%, 71%, and 70%, and the corresponding r_2 are 85%, 326%, and 557%. Obviously, the gain ratio in the case of IPOR is the biggest, followed by the corresponding values for EOR and MOR. This could be resulted from the mass transport effect. It is generally accepted that the smaller molecular size and higher molecular polarity could lead to an easier mass transfer [22]. For the investigated alcohols, their molecular size is in

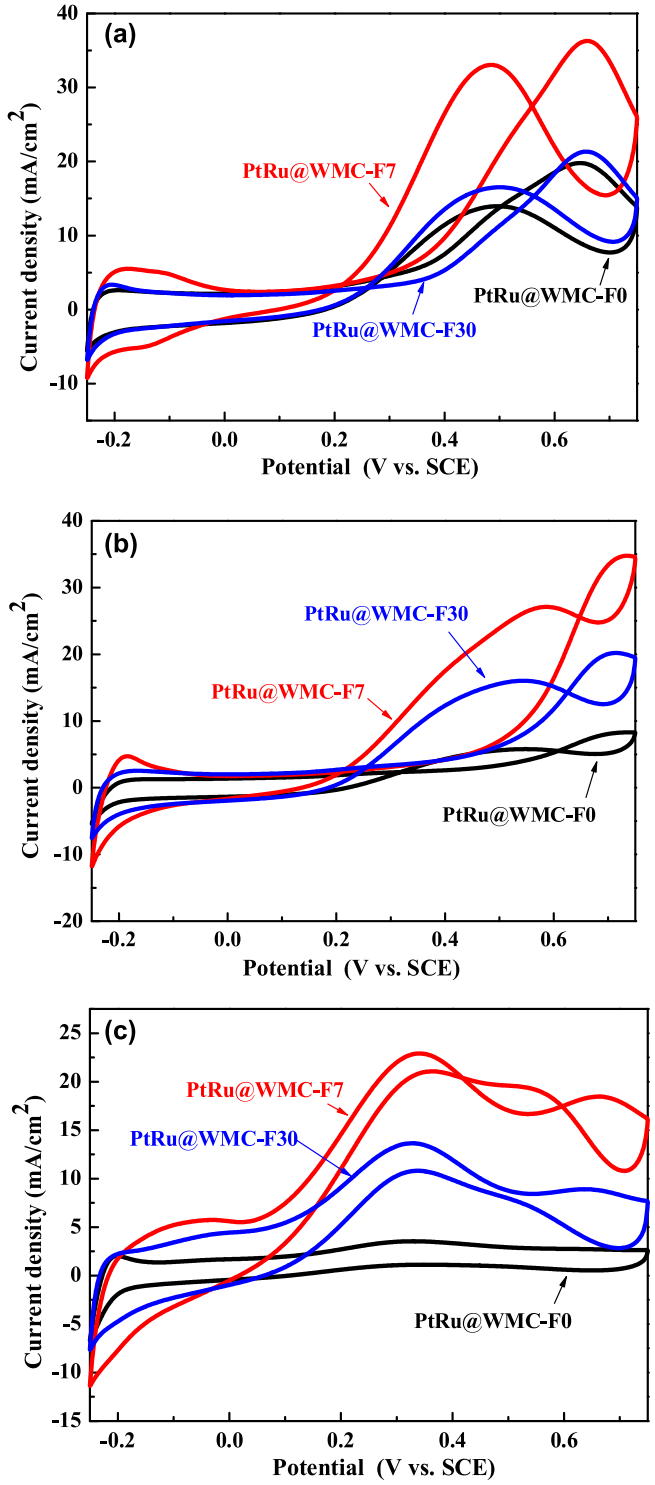

Fig. 7. CVs of alcohol electrooxidation on PtRu@WMC-F0, PtRu@WMC-F30, and PtRu@WMC-F7 in the electrolytes of 0.5 mol/L H_2SO_4 + 1.0 mol/L CH_3OH (a), 0.5 mol/L H_2SO_4 + 1.0 mol/L C_2H_5OH (b), and 0.5 mol/L H_2SO_4 + 1.0 mol/L $(CH_3)_2CHOH$ (c). Scan rate: 50 mV/s.

the order of $CH_3OH < C_2H_5OH < CH_3CH(OH)CH_3$, while the molecular polarity order is $CH_3OH > C_2H_5OH > CH_3CH(OH)CH_3$. Consequently, it can be inferred that the mass transfer order is $CH_3OH > C_2H_5OH > CH_3CH(OH)CH_3$. As a result, the mass transfer effect caused by the pore diameter of WMCs becomes prominent for $CH_3CH(OH)CH_3$ electrooxidation.

Table 3. Electrochemical activity of PtRu@WMC-F0, PtRu@WMC-F30 and PtRu@WMC-F7 in different electrolytes.

Samples	Peak current density of alcohol oxidation, I_p (mA/cm^2)		
	I_p (MOR)	I_p (EOR)	I_p (iPOR)
PtRu@WMC-F7	36.4	34.5	22.9
PtRu@WMC-F30	21.5	20.2	13.5
PtRu@WMC-F0	19.7	8.1	3.5
r_1(%)	69	71	70
r_2(%)	85	326	557

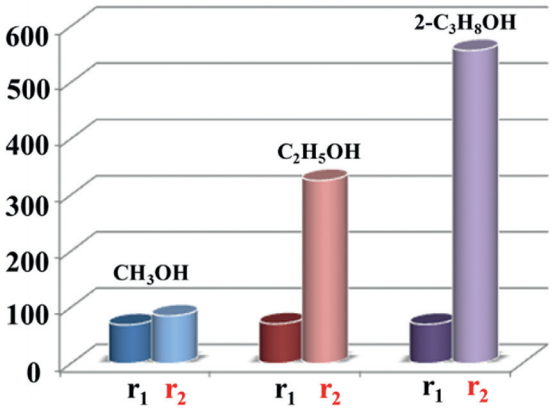

Fig. 8. Comparison of the electrochemical activity of PtRu@WMC-F0, PtRu@WMC-F30 and PtRu@WMC-F7 in different electrolytes.

4. Conclusions

In summary, we have demonstrated that the pore diameter of the supporting material (WMCs) displays a significant role in the accessibility of PtRu nanoparticles and thus their electrocatalytic activity. WMCs with $D_p > 2d_{Pt}$ provide PtRu with higher electrochemical activity at orders of magnitude, especially in the case of isopropanol electrooxidation with a bigger molecular while a small polarization as the reactant. Specifically, the IPOR peak current density arrives at 22.9 mA/cm^2 on PtRu@WMC-F7, compared with 3.5 mA/cm^2 on PtRu@WMC-F7, with a gain ratio of 557%. This priority mainly benefits from the bigger pore diameter of WMC-F7. Considering the significantly improved performance by just adjusting the pore diameter of the supporting materials, we hope that the present work will raise new interests in the role of the pore diameter of porous materials in the electrochemical reactions.

Acknowledgments

This work was supported by the National Natural Science Foundation of China (no. 91434106).

References

[1] S.K. Kamarudin, F. Achmad, W.R.W. Daud, Int. J. Hydrogen Energy 34 (2009) 6902–6916.
[2] K. Vignarooban, J. Lin, A. Arvay, S. Kolli, I. Kruusenberg, K. Tammeveski, L. Munukutla, A.M. Kannan, Chin. J. Catal. 36 (2015) 458–472.
[3] G. Wang, T. Takeguchi, E.N. Muhamad, T. Yamanaka, W. Ueda, Int. J. Hydrogen Energy 36 (2011) 3322–3332.
[4] J.G. Guo, G.Q. Sun, S.G. Sun, S.Y. Yan, W.Q. Yang, J. Qi, Y.S. Yan, Q. Xin, J. Power Sources 168 (2007) 299–306.
[5] R.G. Freitas, E.P. Antunes, E.C. Pereira, Electrochim. Acta 54 (2009) 1999–2003.
[6] X.H. Jian, D.S. Tsai, W.H. Chung, Y.S. Huang, F.J. Liu, J. Mater. Chem. 19 (2009) 1601–1607.
[7] M. Soszko, M. Łukaszewski, Z. Mianowska, A. Czerwińsk, J. Power Sources 196 (2011) 3513–3522.
[8] B. Li, D.C. Higgins, S. Zhu, H. Li, H. Wang, J. Ma, Catal. Commun 18 (2012) 51–54.
[9] S. Wsamus, A. Kuver, J. Electroanal. Chem. 461 (1999) 14–31.
[10] P. Sivakumar, V. Tricoli, Electrochim. Acta 51 (2006) 1235–1243.

[11] W. Xing, S.Z. Qiao, R.G. Ding, F. Li, G.Q. Lu, Z.F. Yan, H.M. Cheng, Carbon 44 (2006) 216–224.
[12] H.J. Liu, W.J. Cui, L.H. Jin, C.X. Wang, Y.Y. Xia, J. Mater. Chem. 19 (2009) 3661–3667.
[13] S.H. Liu, C.C. Chiang, M.T. Wu, S.B. Liu, Int. J. Hydrogen Energy 35 (2010) 8149–8154.
[14] X.Z. Cui, J.L. Shi, L.X. Zhang, M.L. Ruan, J.H. Gao, Carbon 47 (2009) 186–194.
[15] B. Han, W. Zhou, A. Sayari, J. Am. Chem. Soc. 125 (2003) 3444–3445.
[16] D.C. Wu, Z.H. Li, Y.R. Liang, X.Q. Yang, X.H. Zeng, R.W. Fu, Carbon 47 (2009) 916–918.
[17] S.Q. Song, J. Liu, J. Shi, H. Liu, V. Maragou, Y. Wang, P. Tsiakaras, Appl. Catal. B: Environ. 103 (2011) 287–293.
[18] V. Radmilovic, H.A. Gasteiger, P.N. Ross, J. Catal. 154 (1995) 98–106.
[19] F.H. Yan, X.D. Wang, Y.Y. Zheng, J.F. Shen, J.H. Yuan, A.J. Wang, N. Li, S.T. Huang, Electrochim. Acta 198 (2016) 127–134.
[20] C.X. He, S.Q. Song, J.C. Liu, V. Maragou, P. Tsiakaras, J. Power Sources 195 (2010) 7409–7414.
[21] Y. Wang, S.Q. Song, P.K. Shen, C.X. Guo, C.M. Li, J. Mater. Chem. 19 (2009) 6149–6153.
[22] L.Z. Zhou, T. Wang, N. QuangTrong, J. Li, Y.C. Long, Z.H. Ping, Sep. Purif. Technol. 44 (2005) 266–270.